Simulated Density Currents in Idealized Stratified Environments

CHANGHAI LIU AND MITCHELL W. MONCRIEFF

National Center for Atmospheric Research, Boulder, Colorado

(Manuscript received 26 March 1999, in final form 1 July 1999)

ABSTRACT

The effects of three distinct stratifications on density current dynamics are investigated using a nonhydrostatic numerical model: (i) a stably stratified layer underneath a deep neutrally stratified flow, representing a nocturnal boundary layer over land; (ii) a neutrally stratified layer underlying a deep stably stratified flow, representing a daytime boundary layer; and (iii) a continuously stratified atmosphere.

In the first case, a weak or intermediate stratification decreases the height of density currents and increases the propagation speed. The same result holds in strongly stratified situations as long as the generated disturbances in the neighborhood of the head do not propagate away. Classical density currents occur in weak stratification, multiheaded density currents in intermediate stratification, and multiheaded density currents with solitary wave–like or borelike disturbances propagating ahead of the current in strong stratification.

In the second case, the upper-layer stratification consistently reduces the density-current height and its propagation speed. The simulated system resembles laboratory density currents and is not much affected by the overlying stratification.

Finally, in continuously stratified flow, the effect of stratification is similar to the second case. The density current becomes shallower and moves more slowly as the stratification is increased. The modeled system has the basic features of density currents if the stratification is weak or moderate, but it becomes progressively less elevated as stratification increases. In strong stratification the density current assumes a wedgelike structure.

The simulation results are compared with the authors' previously obtained analytical results, and the physical mechanisms for the effect of stratification are discussed.

1. Introduction

The research reported herein is part of a systematic study aimed at quantifying how atmospheric density currents are distinguished from their laboratory counterparts through the effects of stratification, shear, latent heating, and evaporative cooling. Applications of the work include convection initiation and a physical basis for ''triggering'' convective parameterizations in large-scale numerical models. Note that while density currents (e.g., manifested as downdraft outflows, gust fronts, and sea breezes) are known to be important in the real atmosphere, little attempt has been made to introduce dynamic concepts into convective triggering. An imperative is that complex physical aspects must be reduced to first principles, which is in the spirit of our idealized approach.

A considerable amount of research has been performed on density currents in neutrally stratified fluids employing theory, laboratory experiments, and numerical models (e.g., Benjamin 1968; Droegemeier and Wilhelmson 1987; Simpson 1987; Moncrieff and So 1989; Xu 1992; Xu and Moncrieff 1994; Chen 1995; Liu and Moncrieff 1996a; Xu et al. 1996; Xue et al. 1997; Moncrieff and Liu 1999). However, density currents in a stratified fluid, which is a characteristic of the earth's atmosphere, have received relatively little attention and are less well understood. Using a nonhydrostatic numerical model, Crook and Miller (1985) examined density currents propagating into a surface-based, low-level stable layer underneath a deep neutrally stratified flow. Crook (1986) included stratification overlying the stable layer. A comprehensive nonhydrostatic modeling study of the effect of an ambient low-level stable layer on the evolution of density currents was conducted by Haase and Smith (1989). These studies focused on the formation, structure, and propagation of atmospheric undular bores (''morning glories'') spawned by density currents in strongly stratified situations.

Few modeling studies of density currents in physically more complex circumstances have been conducted. Thorpe et al. (1980) performed numerical simulations for a typical (daytime) atmospheric situation featuring a neutral boundary layer underneath a progressively enhanced stratification to examine the ambient flow effect on the propagation and structure of density currents. The simulation with a similar atmospheric con-

Corresponding author address: Dr. Changhai Liu, National Center for Atmospheric Research, P.O. Box 3000, Boulder, CO 80307-3000. E-mail: chliu@ncar.ucar.edu

dition was made by Droegemeier and Wilhelmson (1986) to investigate the stratification effect on the Kelvin–Helmholtz billows associated with density currents. Bischoff-Gauss and Gross (1989) simulated density currents intruding into either a continuously stratified atmosphere or an atmosphere with an elevated inversion. Raymond and Rotunno (1989) studied the nonlinear response of an idealized stratified atmosphere to imposed cooling near the surface. They showed that cooling a stably stratified boundary layer produces very different results from the corresponding neutral case. In particular, dynamic behavior sometimes resembles a gravity wave rather than a density current. Jin et al. (1996) simulated an observed density current in an environment having a nocturnal inversion and elevated neutral layer, further complicated by wind shear. Density currents flowing through two-fluid and continuously stratified surroundings are also examined via laboratory experiments (Simpson 1987).

In addition to the aforementioned studies, Liu and Moncrieff (1996b) investigated the bulk characteristics of conservative density currents in stratified environments using a steady nonlinear analytic model. In particular, they explored how ambient stratification regulates the height and propagation of density currents subject to the ''flow-force balance'' integral constraint. It was found that stable stratification decreases the height of density currents and increases their propagation speed, whereas latent heating has the opposite effect. This result differs markedly from the classic energy-conserving solution in which the propagation speed of a density current is proportional to its height. This disparity stems from the pressure gradients caused by stratification and latent heating.

Many questions about the effects of stratification on the evolution and structure of density currents remain unanswered due to a lack of systematic investigations. For instance, how do stratification strength and distribution regulate the behavior of density currents? In what circumstances are the analytic models of Liu and Moncrieff (1996b) that omit *transient* gravity waves valid? How do ambient flow and wind shear affect density currents in stratified fluids? To improve our knowledge of such mechanisms, we adopt a numerical approach and concentrate on the following scenarios: (i) a shallow stratified layer with a deep neutral layer above to model nocturnal conditions; (ii) a shallow neutral layer underneath a deep stratified layer to model the daytime environment; and (iii) a continuously stratified atmospheric state. We consider an initially motionless atmosphere in order to simplify the physical interpretation of the simulations.

The design of the numerical experiments is described in section 2, followed by density current simulations in a neutral environment in section 3. Sections 4, 5, and 6 are devoted to the simulated density currents flowing in a low-level stable layer, in a low-level neutral layer, and in a continuously stratified environment, respectively. The results are further discussed in section 7 followed by conclusions in section 8.

2. Numerical experiments

a. Model

We use a two-dimensional version of a nonhydrostatic, anelastic model (Clark 1977). The domain is 280 km wide with a grid length of 100 m. The depth of the domain is 15 km. To resolve the detailed structure of density currents and the associated wave disturbances, the vertical grid has a constant resolution of 50 m below 2 km and is gradually stretched to about 500 m at the highest level. There are 102 grid levels in the vertical. Rigid and free-slip boundary conditions are employed at the top and bottom of the model domain. An open condition is implemented at the lateral boundaries. In addition, a Rayleigh friction absorber is applied to the uppermost 5 km to inhibit the reflection of upward-propagating gravity waves.

b. Experiment design

The model is initialized with a motionless base state and a horizontally homogeneous potential temperature field. The density current is initiated and maintained by imposing a time-invariant cold-air source over a region 5 km wide by 1 km high. The cold reservoir has a sine function distribution in the vertical with a maximum potential temperature deviation of -8 K at the surface, decreasing to zero at 1 km.

We conducted three sets of 2-h-long numerical experiments. The first concerns density currents in a shallow stratified layer beneath a deep neutral layer; the second in a neutrally stratified layer beneath a deep stratified layer; and the third in a continuously stratified fluid. The Brunt–Väisälä frequency

$$N = \sqrt{\frac{g}{\theta}\frac{d\theta}{dz}}$$

defines the ambient stratification.

3. Neutral environment

We start by presenting results for a neutral environment to demonstrate the model's ability to simulate the overall features of laboratory and atmospheric density currents and to intercompare the simulations in various stratified states. Cold air spreads out from both sides of the reservoir driven by the horizontal pressure gradient between the pool and the surroundings (see Liu and Moncrieff 1996a). This establishes two symmetric density currents that travel at about 10 m s^{-1} except during the early formation stage (about 10 min). They do not achieve a completely steady state during the 2-h integration; the propagation speed slightly decreases, and the head height and width progressively increase with

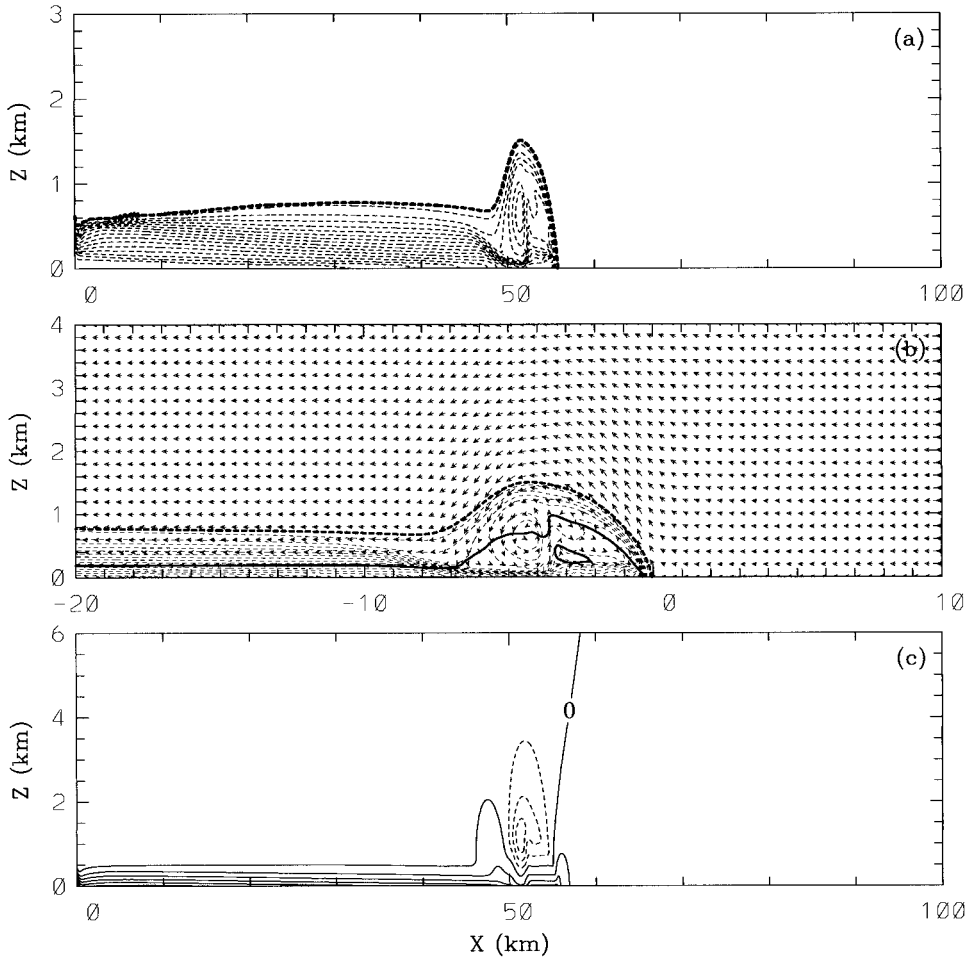

FIG. 1. The density current in the neutral environment at 1.5 h. (a) Potential temperature perturbation (contour starts at −0.1 K with an interval of −0.5 K), (b) system-relative flow and potential temperature perturbation around the leading edge, and (c) pressure perturbation (contour interval is 0.2 mb). The thick dashed line in (a) and (b) is the 0.1 tracer isoline, and the thick solid line in (b) is the zero relative flow isoline.

time. Unless otherwise stated, we focus on the right-moving current, because in an initially motionless environment the left- and right-moving currents are mirror images of each other.

Figure 1 displays the potential temperature perturbation, the system-relative flow, and the pressure perturbation after 1.5 h of integration. Note that the coordinate system in Fig. 1b moves with the density current. Overall, the simulated system resembles a laboratory-generated density current; for example, the cold air in Fig. 1a features the typical elevated head and trailing shallower body. The ambient air flows front to rear in the relative frame of reference (Fig. 1b). Unlike the classical density current models, the cold air is not stagnant relative to its leading edge. Rather, the cold air overturns so that the upper portion flows rearward and the lower portion flows toward the cold front. The strong convergence at the leading edge of the cold air stream causes deep upward motion, which is of primary importance in convection initiation. The positive pressure perturbation prevalent within the cold air is of hydrostatic origin (Fig. 1c), while nonhydrostatic effects are responsible for the negative perturbation around the head as well as the pressure increase ahead of the cold air.

4. A low-level stable layer

The cited modeling studies of density currents propagating in a stable layer focused on borelike or solitary wave–type disturbances spawned by density currents in the highly stratified situation, rather than on density current dynamics per se. This motivated our systematic investigation of the effects of low-level stratification on density currents.

For simplicity, a constant value of N is assumed throughout the stable layer, which extends from the ground to the 1-km level. The ambient potential tem-

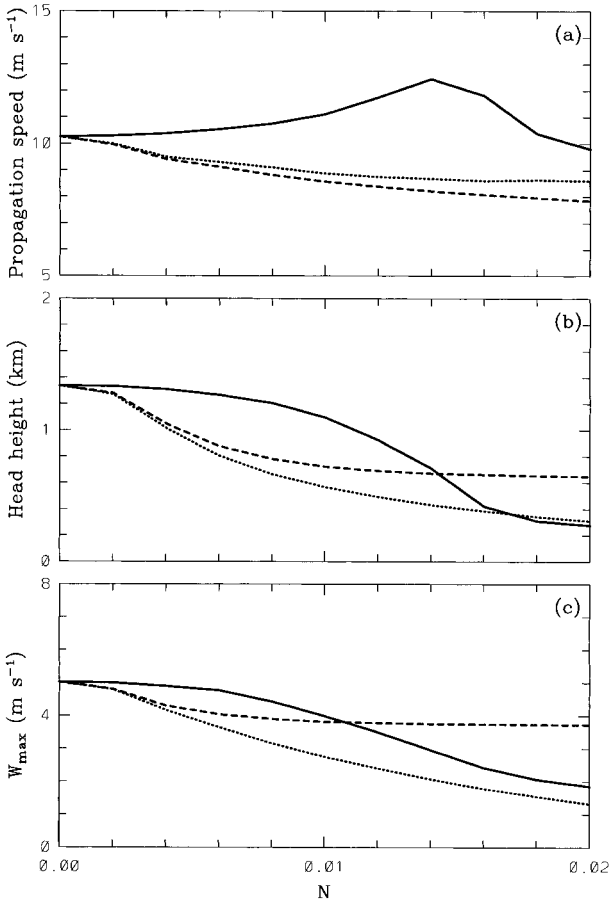

FIG. 2. (a) Variations of the propagation speed with stratification, (b) variations of the head height with stratification, and (c) variation of the maximum vertical velocity with stratification. The solid, dashed, and dotted lines correspond to the low-level stable-layer case, the low-level neutral-layer case, and the continuously stratified case, respectively.

perature increases exponentially with altitude within the stable layer and is constant above:

$$\theta(z) = \begin{cases} \theta_0 \exp\left(\dfrac{N^2}{g} z\right), & z \le 1000 \text{ m} \\ \theta_0 \exp\left(\dfrac{1000N^2}{g}\right), & z > 1000 \text{ m}, \end{cases} \quad (1)$$

where $\theta_0 = 300$ K is the surface potential temperature.

It is difficult to unambiguously determine the cold outflow boundary in a stratified environment in terms of temperature perturbations that can be due to the cold air in the density current, to mechanical lifting, or to gravity waves. Therefore, we use a passive tracer to identify air originating from the cold reservoir. Based upon the neutral environment result shown in Fig. 1, the tracer isoline of 0.1 defines the interface between the air mass from the reservoir and the environmental air. Its intersection with the surface determines the location of the cold front, which is used to determine the propagation speed of density currents and the relative flow structure.

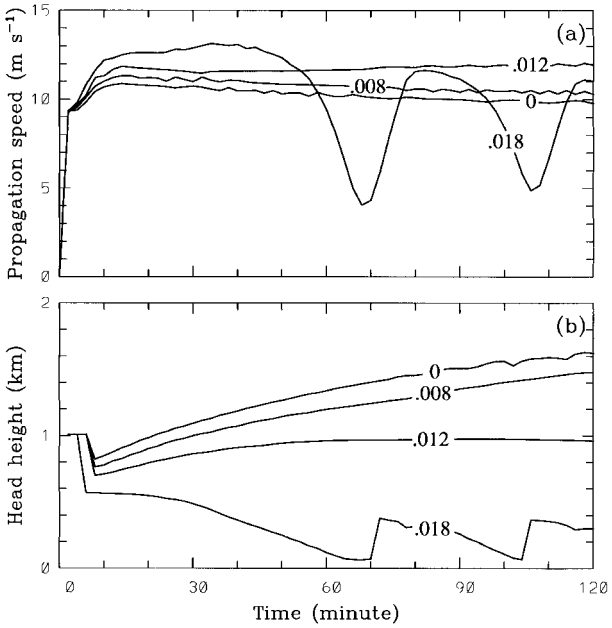

FIG. 3. Evolution of (a) propagation speed and (b) head height for various stratifications in the low-level stable layer.

a. General results

Figure 2 shows the time averages of propagation speed of the density current, the head height, and the maximum vertical velocity for static stabilities ranging from neutral ($N = 0$) to very stable ($N = 0.02$ s^{-1}). The temporal average is taken after the outflow from the reservoir becomes a density current (about 10 min into simulation). The head height refers to the foremost head when multiple heads occur but may also represent the mean height of several short-lived heads as demonstrated later. The mean propagation speed (Fig. 2a) increases with stratification, reaching a maximum of 12.4 m s^{-1} at $N = 0.014$ s^{-1} and then decreases. The transition is due to a dramatic structural change. In contrast, the head height (Fig. 2b) displays a continual reduction as stratification is enhanced. Therefore, the impact of stratification on head height is opposite from that on propagation speed when $N \le 0.014$ s^{-1}.

The maximum vertical velocity is a measure of the potential of density currents for initiating convection. As indicated in Fig. 2c, vertical velocity decreases as the static stability increases, a result consistent with the variation of head heights and the effect of stratification. The maximum vertical velocity, which usually occurs near the leading edge of density currents, is due to mechanical forcing. In strongly stratified situations, however, significant vertical motions can occur far ahead of

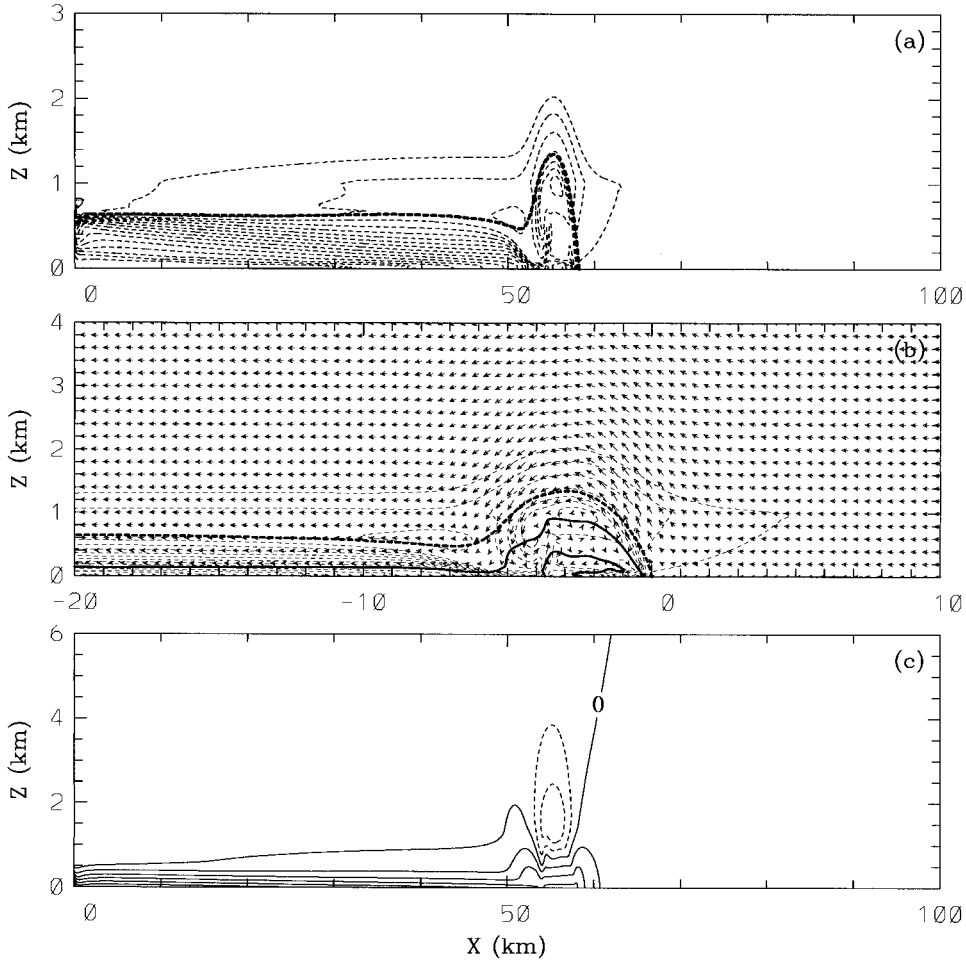

FIG. 4. As in Fig. 1 but for a low-level stable layer with $N = 0.008\ s^{-1}$.

the density current and are due to solitary wave–type disturbances.

In terms of the cold-air outflow, three distinct regimes can be identified, namely classical density currents (i.e., an elevated head trailing with a shallower body) in weak stratification corresponding to $N \leq 0.01\ s^{-1}$, variants of classical density currents (i.e., multiheaded currents) in intermediate stratification for $0.01\ s^{-1} < N \leq 0.014\ s^{-1}$, and multiheaded density currents with propagating solitary waves (bores) in strong stratification for $N \geq 0.016\ s^{-1}$. It should be pointed out that the stratification thresholds vary with the cold-air source strength.

b. Weak stratification

The case of $N = 0.008\ s^{-1}$ demonstrates density-current behavior in the weakly stratified situation. The evolution of the propagation speed and head height of the density current are presented in Fig. 3. Compared to neutral stratification, the effect of weak stratification increases the propagation speed but lowers the head height. The relatively low head is anticipated in stable stratification, but the increase in propagation speed contradicts classical theory (Benjamin 1968) where the propagation speed of a density current is directly proportional to its height. The reason for this contradiction will be explained later in terms of the pressure field. Another notable aspect is that the head becomes progressively elevated, implying that the system fails to reach a steady state, similar to the neutral case. On average, the propagation speed is increased by about 5%, and the height is reduced by about 10% for Brunt–Väisälä frequencies in the range $0 \leq N \leq 0.008\ s^{-1}$. Another common property is that the propagation speed is a weak function of distance from the cold-air source—the farther the outflow moves, the slower it propagates.

Figure 4 displays the potential temperature deviation relative to the environment, the flow in a reference frame moving with the density current, and the pressure perturbation at 1.5 h. The negative perturbation in Fig. 4a is characterized by a head with a depth of about 2 km, followed by a body with a depth of over 1 km. Both are deeper than in the neutral case. Unlike the neutral situation, however, the potential temperature perturba-

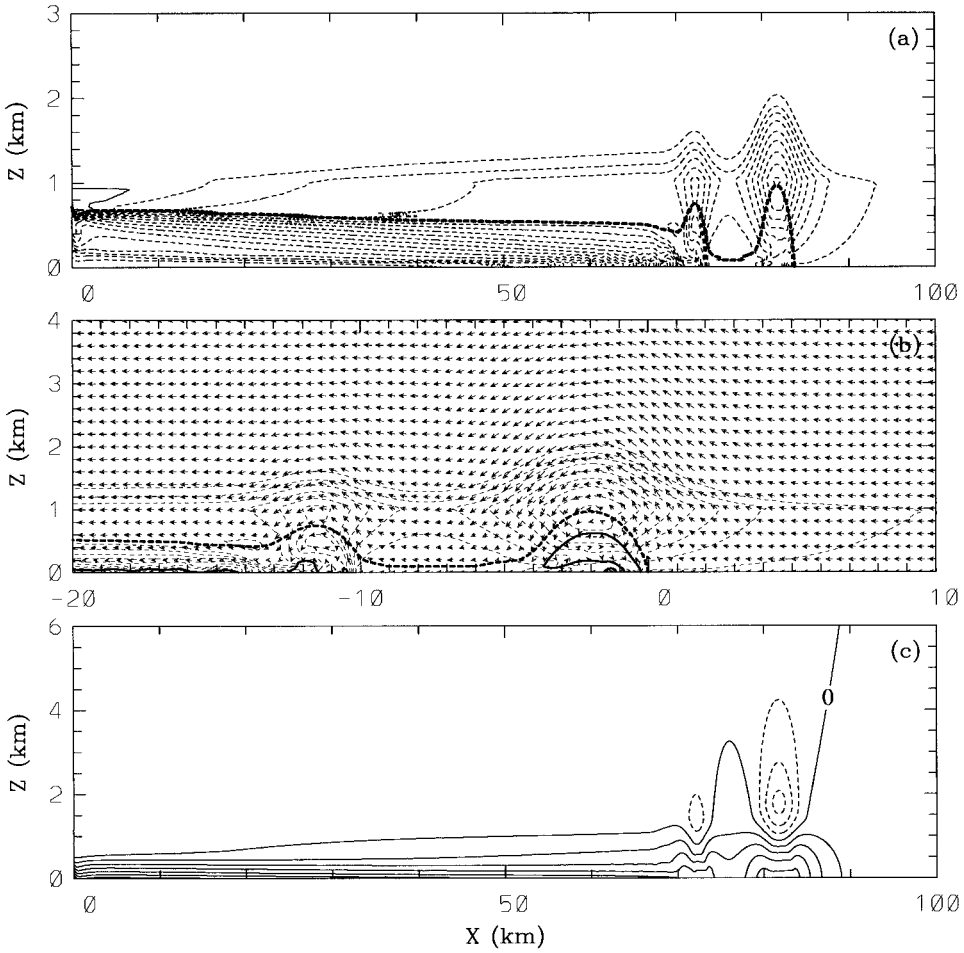

FIG. 5. The density current for a low-level stable layer with $N = 0.012\ s^{-1}$ at 2 h. (a) Potential temperature perturbation (contour starts at -0.1 K with an interval of -0.5 K), (b) system-relative flow and potential temperature perturbation around the leading edge, and (c) pressure perturbation (contour interval is 0.2 mb). The thick dashed line in (a) and (b) is the 0.1 tracer isoline, and the thick solid line in (b) is the zero relative flow isoline.

tion consists of two distinct components. One is rooted to the surface and consists of density-current air. The other, situated above and ahead of the head, is due to adiabatic cooling of mechanically lifted ambient air from ahead of the current. These two components are separated by the 0.1 tracer contour (the thick dashed line in the figure). The cold air defined by the tracer identifies the basic feature of density currents—an elevated head roughly 1.4 km high with a trailing body about 0.6 km high. In comparison with the neutral environment, the heights of head and body are reduced by stable stratification.

The potential temperature perturbation due to the adiabatically cooled ambient air could be misinterpreted as a part of cold outflow were the outflow boundary measured solely in terms of a temperature perturbation. Observational analyses may be prone to this misinterpretation, and this issue has been discussed by Smith et al. (1995). The adiabatically generated potential temperature perturbations affect the density-current propagation speed through its impact on the hydrostatic pressure.

The relative flow in Fig. 4b resembles the neutral case; that is, a surface-based forward flow within the density current overlaid by a widespread reverse flow. In spite of the stable stratification, significant mechanically driven upward motion occurs in the neighborhood of the leading edge. This upward motion penetrates deeply because of the deep neutral environment. The pressure perturbation in Fig. 4c also has a distribution similar to the neutral case; the hydrostatically generated positive pressure dominates in the lowest kilometer whereas the relatively weak negative pressure of a nonhydrostatic origin prevails above and around the head. The primary difference between the neutral and the stratified case concerns the slightly stronger and deeper positive pressure perturbation due to the adiabatic cooling of upward-displaced ambient air. The larger pressure gradient at the leading edge of the density current in

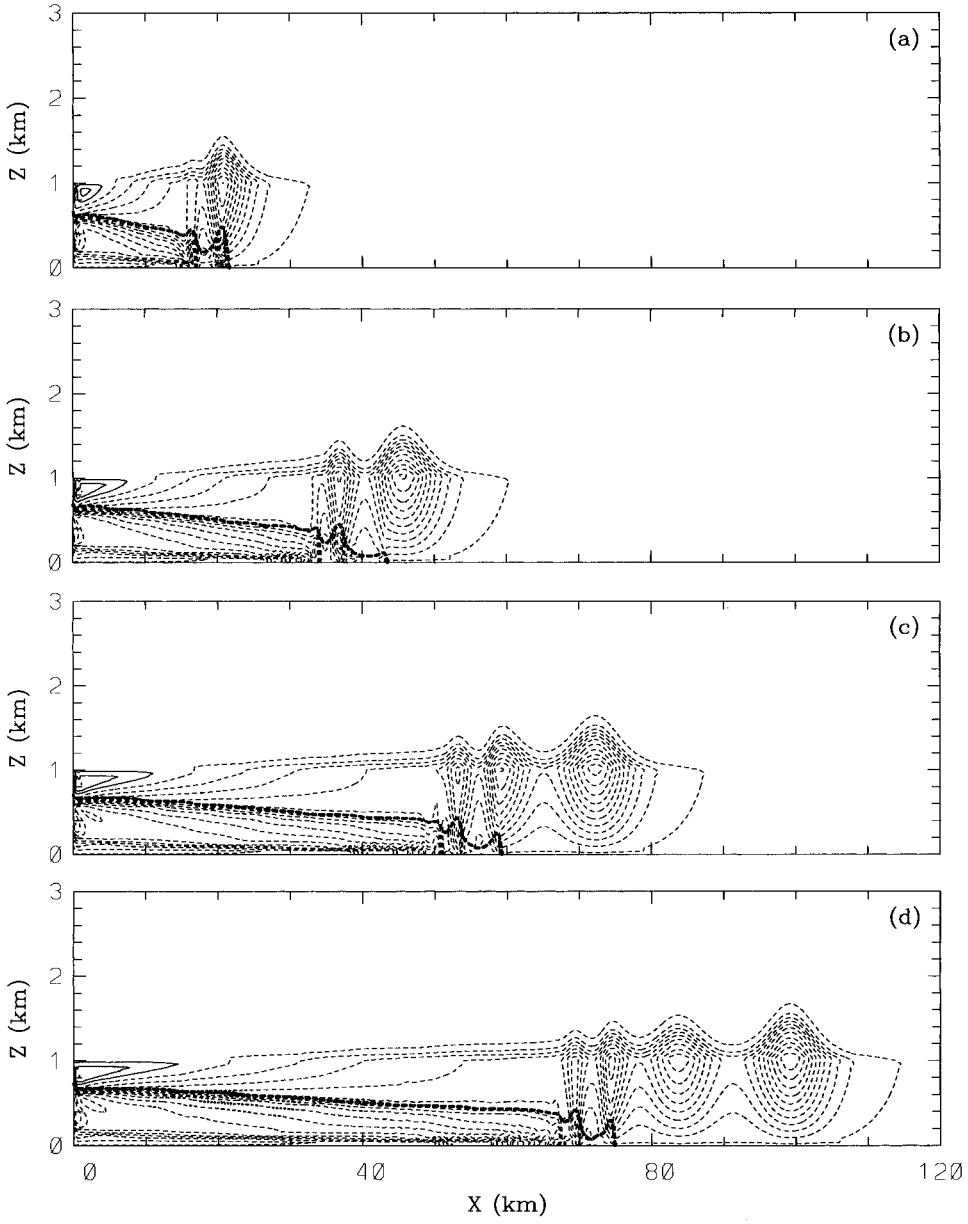

FIG. 6. Potential temperature perturbation for a low-level stable layer with $N = 0.018$ s^{-1}: (a) 0.5 h, (b) 1 h, (c) 1.5 h, and (d) 2 h. Contour starts at -0.1 K with an interval of -0.5 K. The thick dashed line is the 0.1 tracer isoline.

the stratified case accounts for the faster propagation, which is, in turn, responsible for the weaker feeder flow.

c. Intermediate stratification

The case of $N = 0.012$ s^{-1} represents a stratification of intermediate strength. Throughout the simulation, the propagation speed is consistently larger than in either the neutral or the weakly stratified case, whereas the head is shallower (Fig. 3). After a density current develops, the propagation speed varies little. The head height steadily increases, reaching a peak value of 0.96 km at about 50 min, and remains virtually unchanged thereafter.

Figure 5 displays the potential temperature perturbation, the system-relative flow, and the pressure perturbation at the end of the integration. The multiheaded structure is the striking feature. During the first hour, the cold outflow has the characteristic properties of classical density currents and is comparable to the neutral and weakly stratified situations (not shown), even though the cold-air feeder flow does not continuously extend into the head region. At about 1.5 h a second head is initiated and subsequently evolves. The two

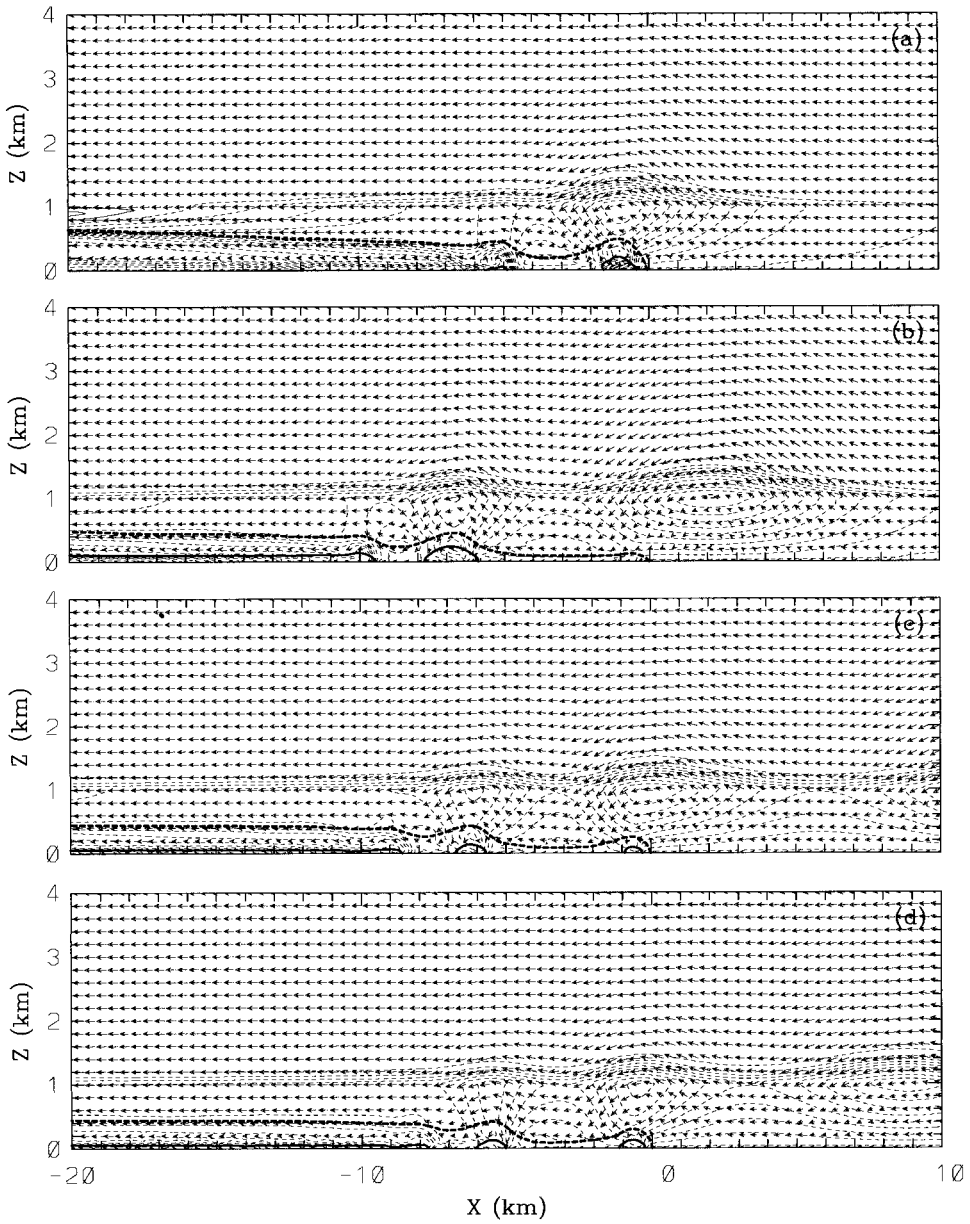

FIG. 7. As in Fig. 6 but for the relative flow and potential temperature perturbation around the leading edge. The thick solid line is the zero relative wind isoline.

heads progressively separate. Nevertheless, by the end of the simulation the front head remains connected to the cold air as revealed in Fig. 5a. It is significant that a multihead structure also occurs in a neutrally stratified but sheared environment (Liu and Moncrieff 1996a). In other words, its presence is not unique to a stratified environment.

As anticipated, the potential temperature perturbation associated with the adiabatic cooling becomes progressively more significant as the stratification increases. The adiabatic cooling generates cold-air domes or solitary wave–like disturbances that envelop the heads, and more extensive negative potential temperature anomalies over the trailing body. The adiabatic cooling is detectable several kilometers upstream of the leading edge.

Unlike the situation in neutral and weak stratification, the rear-to-front relative flow (Fig. 5b) intermittently feeds the leading head due to its swift movement. The rear head grows because it moves slower and can therefore be continuously fed from the cold pool. Because of the strong stratification, the adiabatic cooling overcompensates the reduction of the negative potential temperature deviation within the density current. In particular, the overlapping of the density-current head and the adiabatically produced cooling hump generates noticeable positive pressure perturbations. The pressure gra-

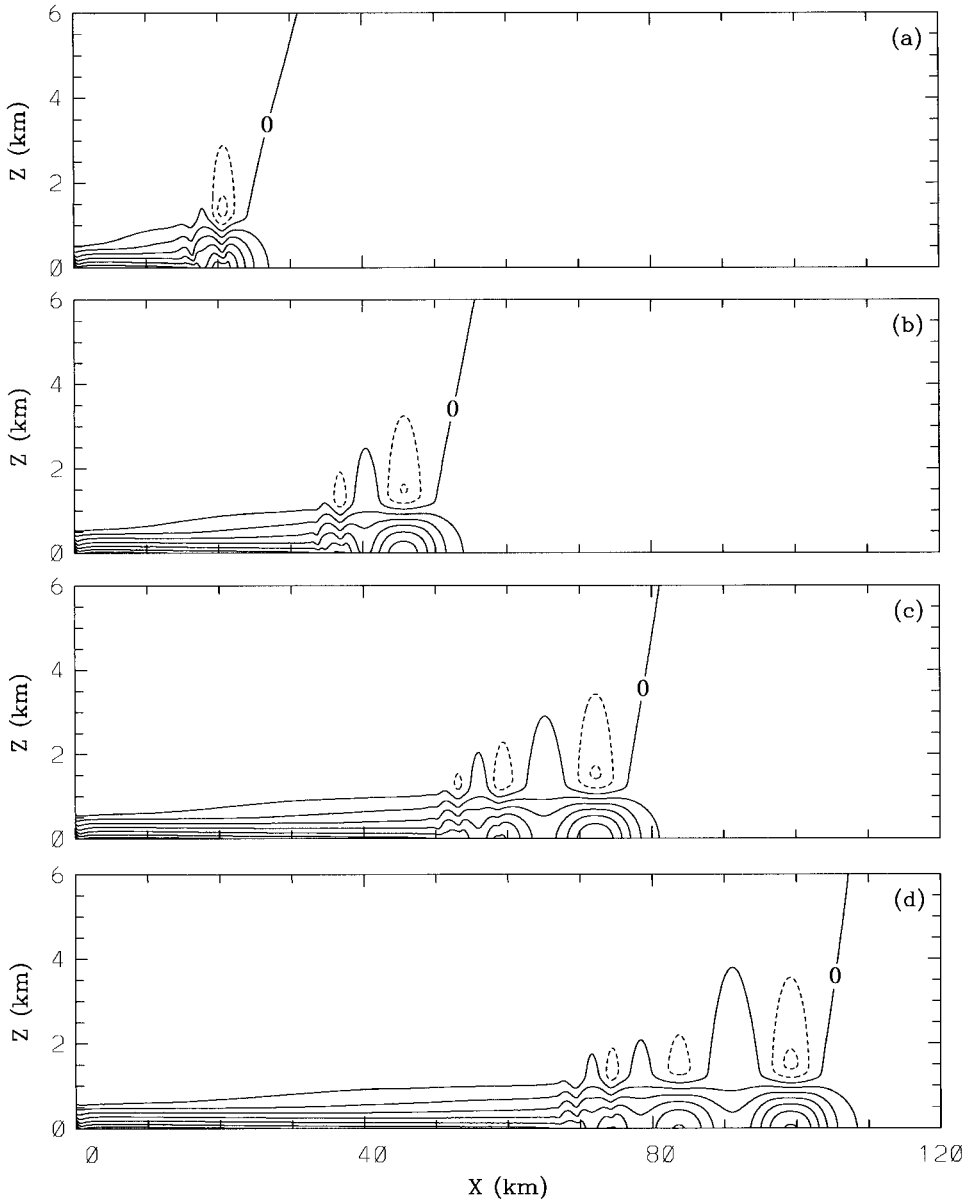

FIG. 8. As in Fig. 6 but for the pressure perturbation. Contour interval is 0.2 mb.

dient between the current and the environment (Fig. 5c) effects a larger propagation speed than either the neutral case or the weakly stratified case. It is the relatively swifter propagation of the leading (foremost) head that is responsible for the disconnection of the cold-air supply and the occurrence of the rear head.

d. Strong stratification

The case of $N = 0.018\ s^{-1}$ illustrates the density-current behavior in strong stratification. The evolution of both the propagation speed and the head height exhibit strong oscillations (Fig. 3). Nevertheless, the current head is consistently the lowest among the examples presented thus far. We will show that the faster (slower) movement occurs when the borelike disturbance is coupled with (decoupled from) the head.

Figures 6–8 present the potential temperature perturbation, the relative flow, and the pressure perturbation at 0.5, 1, 1.5, and 2 h. This set of simulations demonstrates the evolution of the cold outflow and the attendant wave disturbances. At 0.5 h, the density current exhibits a two-headed structure (Figs. 6a and 7a). The heads are localized in the sense that they are *shallower* than the body. The striking adiabatically generated solitary wave–like disturbance is coupled to the leading head. The mutual contribution of the density current and the adiabatically produced cooling establishes large hor-

izontal pressure gradients (Fig. 8a), causing a fast translation of the density current (Fig. 3). The trailing body has a very steady structure, and overlaps with the adiabatic cooling. Its depth is inversely proportional to the distance from the cold-air source. At this moment, the relative flow (Fig. 7a) is almost totally rearward within the density current; therefore, the feeder flow that transports cold air toward the leading edge is absent in contrast to the other cases.

Unlike the moderately stratified case, the coupling of the density-current head with the adiabatic cooling bulge is a transient feature. The disturbance gradually becomes separated from the leading head as indicated in Figs. 6b and 7b. This decoupling is accompanied by a dramatic transition of the propagation speed and the head height (see Fig. 3). As a result, the foremost head at 1 h is barely discernible, and the leading current assumes a distinctive wedgelike shape. At this time the second head is mature and a third head begins to develop. The shallow leading current, together with the displacement of the adiabatic cooling above, causes a substantial reduction in the propagation speed. In contrast, the trailing head moves much faster because of its strong coupling with the adiabatic cooling. It eventually catches up with the foremost head, which accelerates the density-current propagation speed. Figure 7b shows a rear-to-front relative flow near the surface, which is a result of the deceleration of the system, but it does not reach the leading edge.

By 1.5 h, the disturbance initiated by the first head has moved more than 10 km from the leading edge (Figs. 6c and 7c). The second solitary wave–like disturbance begins to move away from the foremost head, and the density-current propagation speed begins to decrease. During the following half an hour, a similar cycle is repeated, corresponding to the development of a new head and takeover of the foremost head by the trailing one (Figs. 6d and 7d). In total, four heads are produced during the 2-h simulation.

Solitary wave–like disturbances were simulated by Crook and Miller (1985) and Haase and Smith (1989) and are also reported in laboratory experiments (Simpson 1987) and observations (e.g., Clarke et al. 1981; Doviak and Ge 1984). This kind of fast-propagating disturbance produces striking surface pressure surges (Fig. 8), low-level convergence, and vertical motion (Fig. 7), and is a mechanism for initiating convection remote from the parent density current.

5. A low-level neutral layer

We consider a 1-km deep neutral layer overlaid by a deep stratified layer of constant Brunt–Väisälä frequency. The environmental potential temperature is

$$\theta(z) = \begin{cases} \theta_0, & z \le 1000 \text{ m} \\ \theta_0 \exp\left[\dfrac{N^2}{g}(z - 1000)\right], & z > 1000 \text{ m.} \end{cases} \quad (2)$$

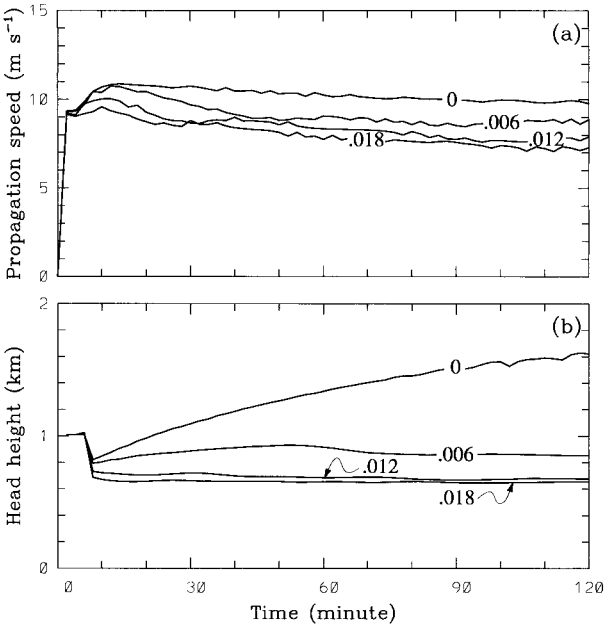

FIG. 9. Evolution of (a) propagation speed and (b) head height for various upper-layer stratifications in the low-level neutral-layer case.

As indicated in Fig. 2, the upper-level stratification reduces both the propagation speed and the density-current head height. This is distinct from the influence of the weak or moderate low-level stratification, which decreases the density-current height but increases the propagation speed. Even weak stratification has a substantial dynamical impact. In contrast, the density-current movement and height are much less sensitive to the stratification variation in the moderately or strongly stratified situation. Overall, the upper-level stratification reduces the maximum vertical velocity and, therefore, the potential of convection initiation by the density-current mechanism. However, the variation with stratification intensity is very small except when the stratification is weak.

Figure 9 presents the evolution of the propagation speed and the head height in simulations with $N = 0.006$ s^{-1}, 0.012 s^{-1}, and 0.018 s^{-1}. The simulation with a neutral stratification is also presented for comparison. The greater the stratification, the smaller the density-current propagation speed and the lower the head height. This behavior holds throughout the 2-h integration. Another notable feature is that the head height displays only minor temporal variation; therefore, the density current is quasi-steady, in contrast to the neutral situation.

The potential temperature perturbations after 1.5 h are shown in Fig. 10. All simulations produce density-current-like systems, but the head becomes progressively less elevated compared to the body. The stratification also lowers the height of the body. As well as the aforementioned influence on the structure and propagation of density currents, upper-level stratification

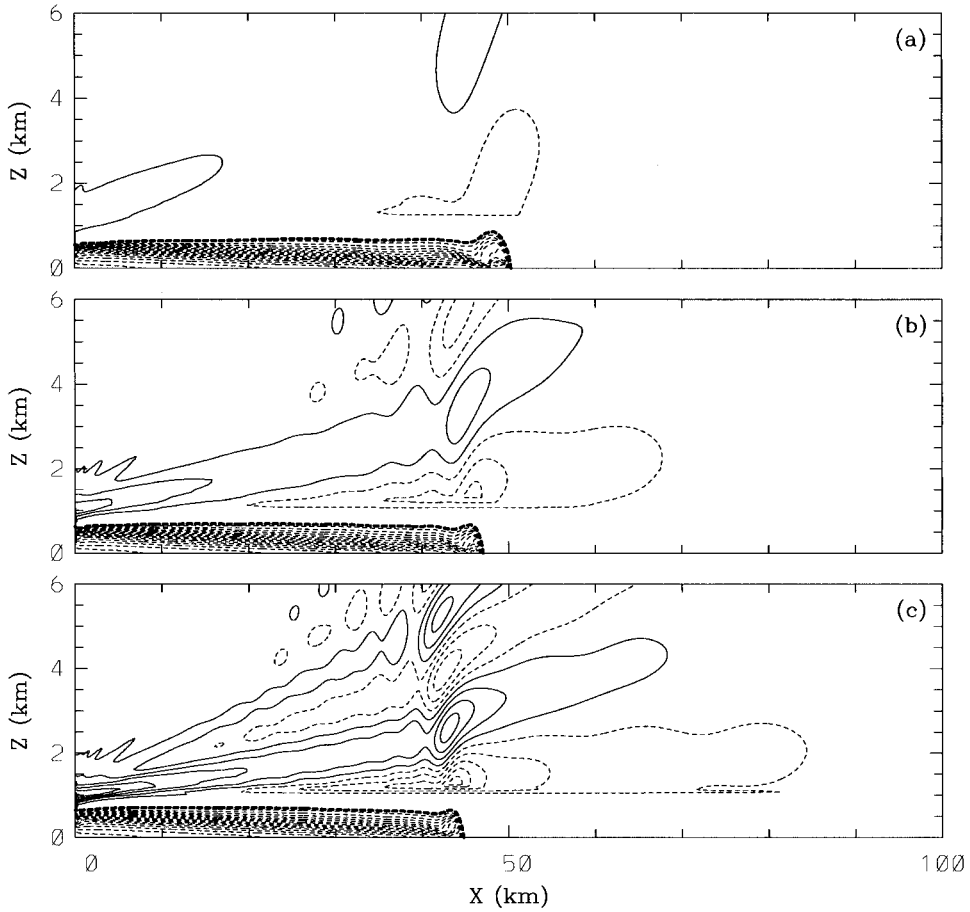

FIG. 10. Potential temperature perturbation for the low-level neutral-layer case at 1.5 h: (a) $N = 0.006$ s^{-1}, (b) $N = 0.012$ s^{-1}, and (c) $N = 0.018$ s^{-1}. Contour interval is 0.5 K with the first solid line at 0.25 K and the first dashed line at -0.25 K. The thick dashed line is the 0.1 tracer isoline.

leads to deep potential temperature perturbations over the cold outflow. This obstacle effect generates gravity waves, whose phase speed and amplitude are proportional to the stratification; thus their effects reach far ahead of the density current, especially in strongly stratified conditions.

The detailed structure of the leading cold outflow and the system-relative flow are depicted in Fig. 11. The flow pattern is similar to that in the neutral case. The rear-to-front feeder flow extends from the source to the leading edge of the outflow. Its depth and intensity are insensitive to the stratification strength. Gravity waves are discernible in the upper layer. The noticeable difference from the neutral case is the absence of a closed circulation (rotor) within the density-current head. Also, upper-layer stratification reduces the height and length of the head.

The corresponding pressure perturbation field is displayed in Fig. 12. Stratification reduces the pressure perturbation and the accompanying horizontal gradients around the leading edge, consistent with a decrease in the propagation speed. The negative pressure perturbation around the head is less significant than in the neutral case. The deep but weak perturbations over and ahead of the density current are gravity waves.

6. Continuously stratified environment

The ambient potential temperature has an exponential distribution,

$$\theta(z) = \theta_0 \exp\left(\frac{N^2}{g} z\right). \tag{3}$$

In general, the influence of stratification resembles that in the low-level neutral layer case; it reduces both the propagation speed and the head height (Fig. 2). This dependence progressively decreases as stratification increases. In fact, the mean propagation speed is almost unchanged when $N > 0.012$ s^{-1}. The head height is more sensitive to the variation of stratification; for instance, it is reduced by roughly 40% when the stratification varies from neutral to $N = 0.006$ s^{-1}, whereas the propagation speed is reduced by only 10%.

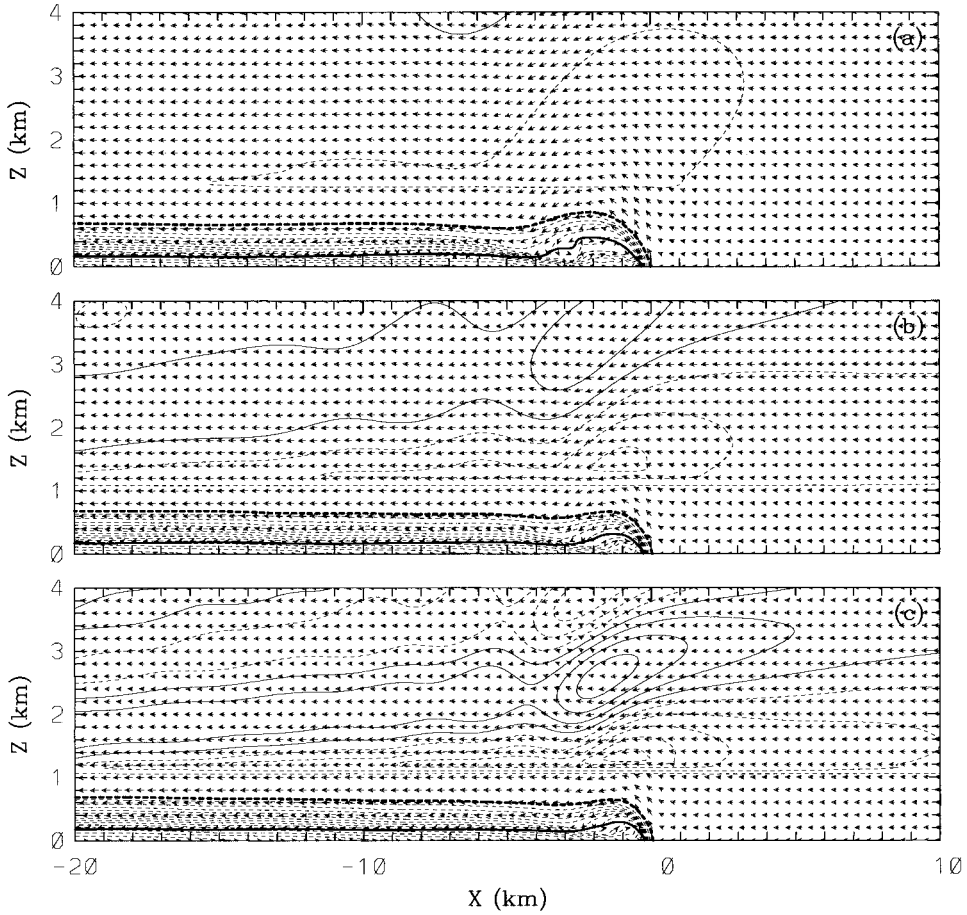

FIG. 11. As in Fig. 10 but for the relative flow and potential temperature perturbation around the leading edge. The thick solid line is the zero relative wind isoline.

Stratification decreases the maximum vertical velocity, as in the other two scenarios. For a given value of N, the continuously stratified case always corresponds to the smallest maximum vertical velocity. The variation of the maximum vertical velocity closely follows that of the head height because the latter is a measure of the mechanical forcing by density currents.

Figure 13 displays the evolution of the propagation speed and outflow head height for weak ($N = 0.004$ s^{-1}), moderate ($N = 0.01$ s^{-1}), and strong stratification ($N = 0.016$ s^{-1}), as well as for the neutral case. In general, the propagation speed changes little and head height is almost constant in the moderately and strongly stratified situations. The head is consistently lower in stronger stratification. In contrast, the propagation speed exhibits a more complicated evolution, despite the fact that stronger stratification always corresponds to faster propagation (Fig. 2).

The potential temperature perturbation fields after 1.5 h are shown in Fig. 14. The stratification effect is comparable to the neutral lower-layer case discussed in the last section. It modifies the outflow morphology by flattening both the head and the trailing body. In comparison, the stratification has a much more significant influence on the head than on the body. For the weakly and moderately stratified cases, the outflow retains the fundamental characteristics of classical density currents in terms of the tracer distribution, although the head is much less raised than in the neutral case. As in the neutral lower-layer situation, the mutual action of mechanical lifting and gravity waves causes salient potential temperature perturbations over and ahead of the density current. Because the gravity wave propagation speed is proportional to the stratification, perturbations can extend far ahead of the density-current system in moderately or strongly stratified environments.

The detailed thermodynamic and kinematic characteristics around the density-current head are shown in Fig. 15. The potential temperature perturbation clearly reveals that the weak or moderate stratification does not greatly change the density-current structure. However, the strong perturbations caused by the gravity wave activity and mechanical lifting overlap the current, making it impossible to distinguish between these distinct dynamical mechanisms in terms of potential temperature perturbations alone. The outline of the outflow deter-

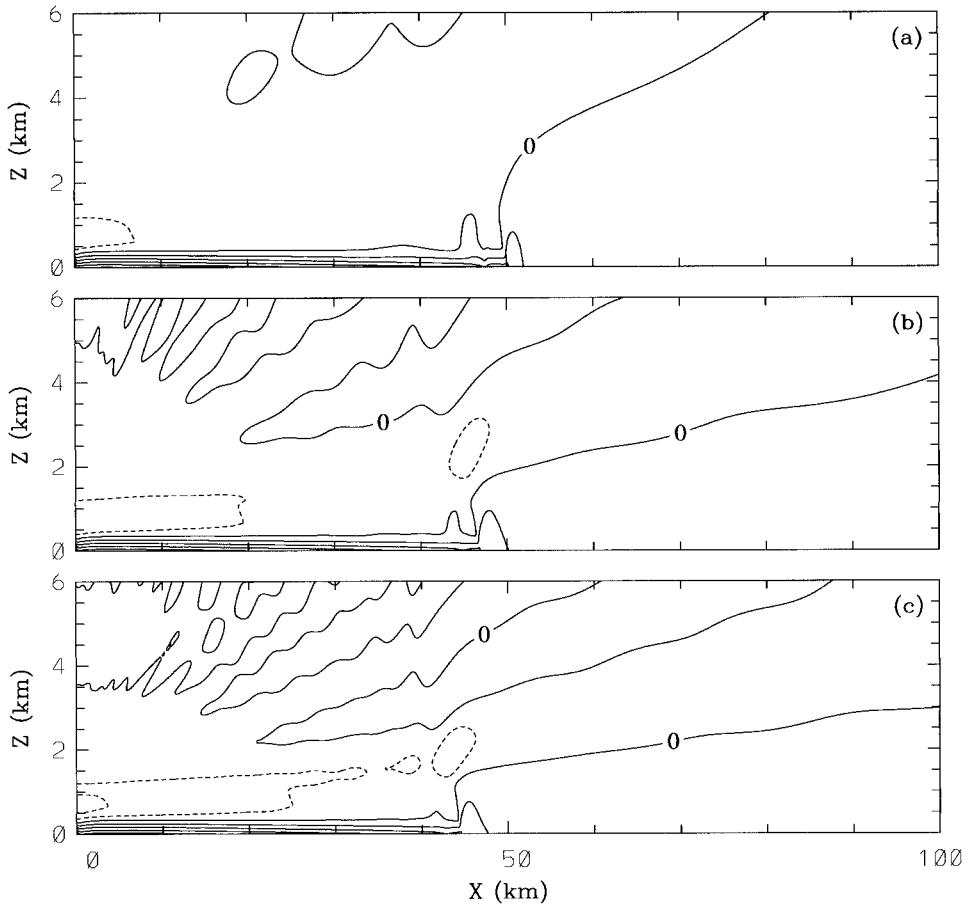

FIG. 12. As in Fig. 10 but for the pressure perturbation. Contour interval is 0.2 mb.

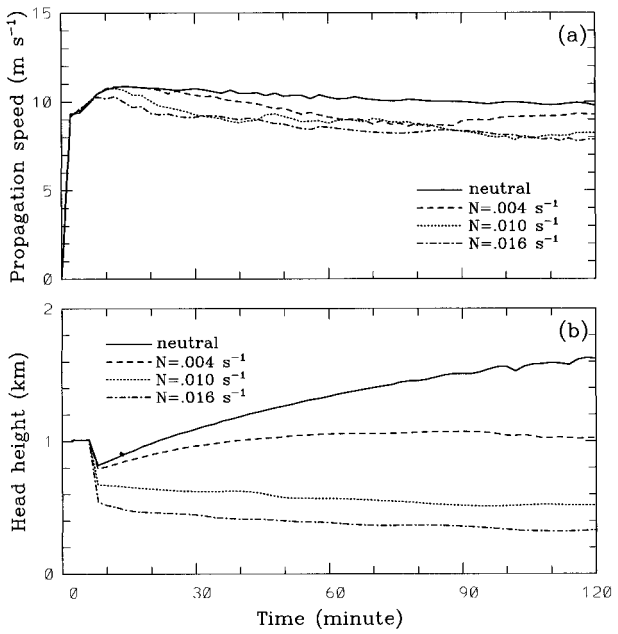

FIG. 13. Evolution of (a) propagation speed and (b) head height for various stratifications in the continuously stratified case.

mined from the passive tracer exhibits a wedgelike structure in the strongly stratified case. The relative flow is mostly unchanged by the stratification and features a characteristic rear-to-front flow underneath a deep rearward flow. The major structural difference caused by stratification is the weakening or even disappearance of a closed circulation (rotor) within the head.

Figure 16 shows the corresponding pressure perturbation field. Two differences compared to the neutrally stratified case are noteworthy. First, in stratified flow, the negative pressure deviation around the head is considerably reduced and the low pressure center consequently no longer exists, whereas the negative pressure over the density current body is enhanced. Second, gravity waves cause pressure perturbations far ahead of the density current although the low-level positive deviation ahead of the head is the most marked. Thus a pressure rise can be detected long before the arrival of the density current. This gravity wave–generated pressure perturbation decreases the horizontal pressure gradient between the density current and the environment. This accounts for the reduction of propagation speed despite the large surface pressure perturbation within the current.

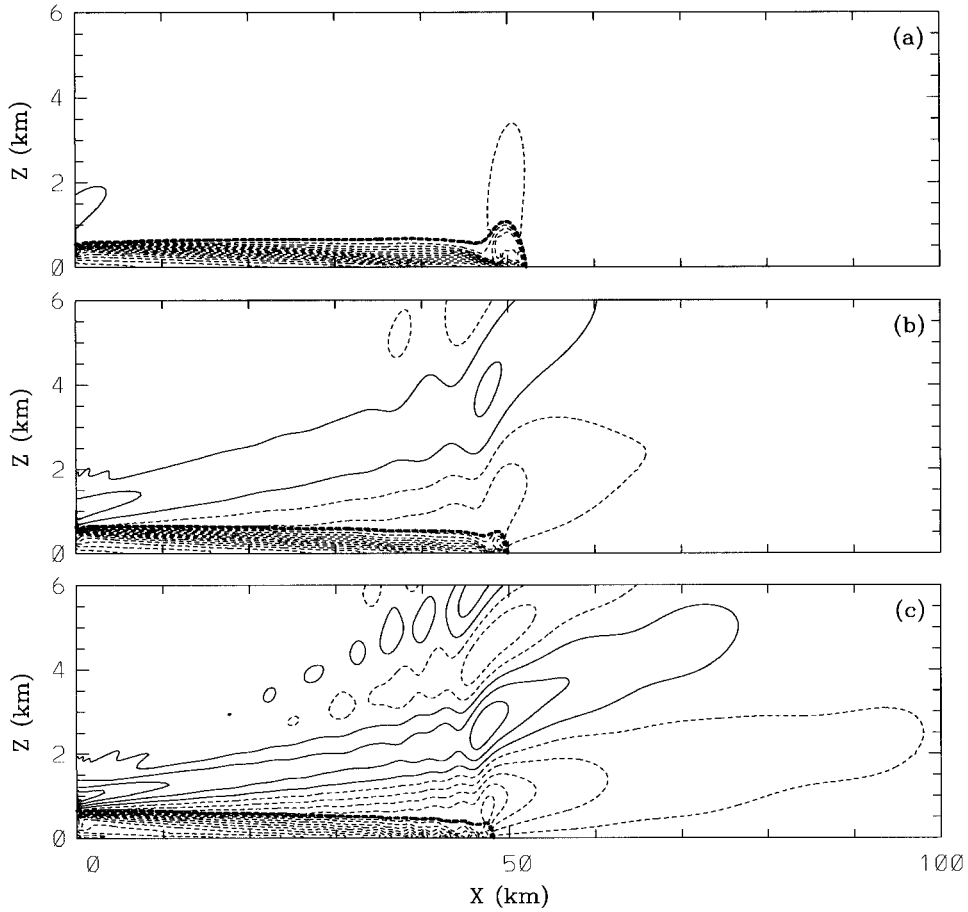

FIG. 14. Potential temperature perturbation for the continuously stratified state at 1.5 h: (a) $N = 0.004$ s^{-1}, (b) $N = 0.01$ s^{-1}, and (c) $N = 0.016$ s^{-1}. Contour interval is 0.5 K with the first solid line at 0.25 K and the first dashed line at -0.25 K. The thick dashed line is the 0.1 tracer isoline.

7. Discussion

a. Physical mechanisms

We identify three mechanisms by which stratification influences density-current dynamics. The first concerns the stabilization effect [negative (positive) buoyancy for an upward (downward) displaced parcel], which suppresses the vertical displacement of ambient air lifted by density currents and also cold air within the current. This process is thought to be responsible for the less elevated head upon including a stable stratification in either the lower layer or the upper layer, or throughout the depth of the computational domain.

The second relates to the negative temperature perturbation generated by the adiabatic cooling of the mechanically lifted ambient air in a stratified flow. This can enhance the surface pressure and the horizontal pressure gradient and is favorable for fast propagation of density currents in stratified flow. This mechanism, suggested by the analytic modeling results of Liu and Moncrieff (1996b), is supported by the simulation results. Figure 17 shows the hydrostatically produced surface pressure by the potential temperature perturbation outside the density current (approximately representing the lower bound of the contributions by the adiabatic cooling) for a typical atmospheric static stability $N = 0.01$ s^{-1}. The surface pressure and the buoyancy-generated pressure within the current are also displayed. Note that the pressure associated with the ambient temperature perturbations is due to both mechanical lifting and gravity wave contributions, which are difficult to separate.

The pressure perturbation due to the adiabatic cooling (and heating) is significant in all three cases shown in Fig. 17, but its horizontal distribution is quite different. For the stable lower-layer case (Fig. 17a), the pressure perturbation is concentrated in the head region and gently decreases rearward. A sharp gradient exists near the leading edge, accounting for the enhanced propagation compared to the neutral environment. The accelerating effect of low-level stratification on density currents has been observed (Physick 1976) and numerically simulated (Haase and Smith 1989), but physically interpreted in terms of reduced friction or the channeling effect of

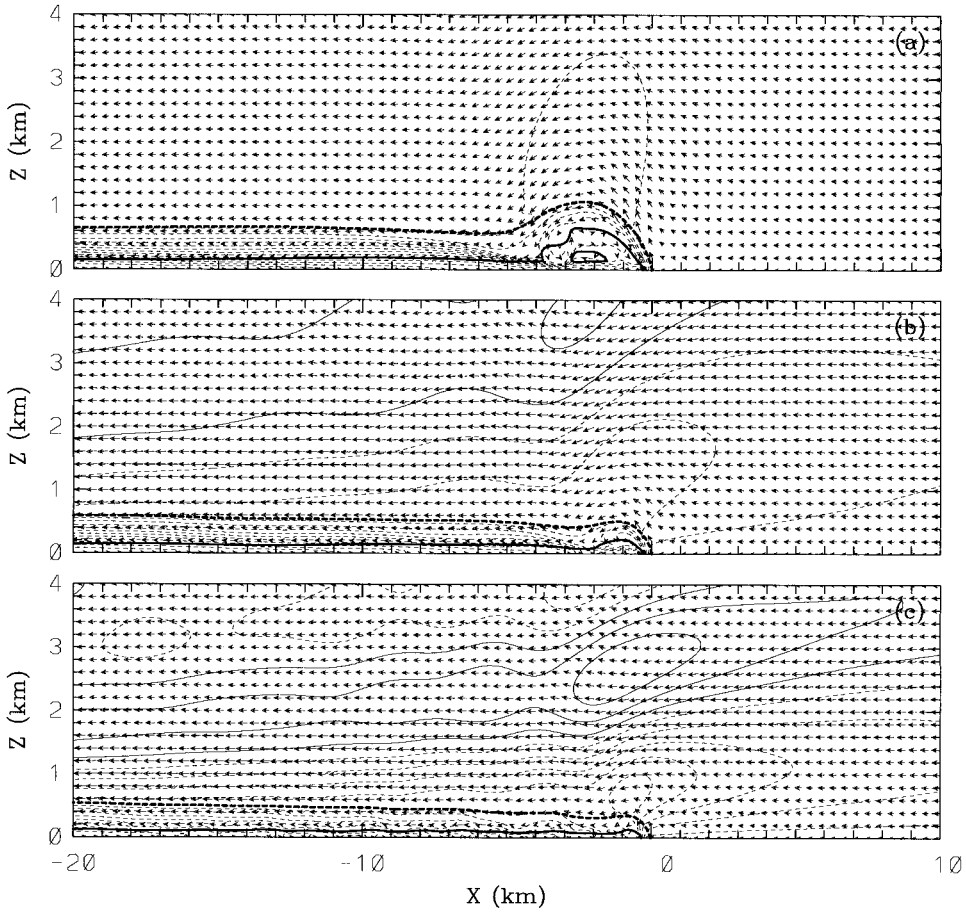

FIG. 15. As in Fig. 14 but for the relative flow and potential temperature perturbation around the leading edge. The thick solid line is the zero relative wind isoline.

the surface-based stable layer. For the neutral lower-layer case (Fig. 17b) and continuously stratified case (Fig. 17c), although the pressure generation associated with adiabatic cooling is a maximum in the vicinity of the head, its effect extends far ahead of the density current. This results in a much more gradual pressure gradient in the neighborhood of the leading edge. The distinct behavior in the stable lower-layer case is attributed to gravity wave trapping.

The third process is related to gravity waves, which produce temperature and pressure perturbations above and ahead of the density current (Fig. 17). Gravity waves affect density currents through energy radiation, but this mechanism does not apply to the stable lower-layer case where the wave trapping occurs. The upward leakage of wave energy can also be blocked if either a low-level jet or an upper-level wind opposing the wave motion is present, or if a midlevel inversion exists (Crook 1988).

b. Comparison with other studies

The effect of ambient stratification on density currents was investigated analytically by Liu and Moncrieff (1996b). Using a nonlinear steady-state model, they examined how a stable stratification regulates the heights of energy-conserving density currents and their propagation speeds. Herein, the response of density currents flowing from a cold-air reservoir in various stratification scenarios is examined. Although a strict comparison is impractical, the analytical results are consonant with the numerical simulations in many aspects. For instance, both analytical and numerical studies illustrate that a density current is less elevated in the stably stratified environment than in the neutral environment. One difference concerns the influence of stratification on propagation. The analytical study shows that a stable stratification increases the propagation speed, whereas in the numerical modeling this is true only for density currents propagating in a low-level stable layer, and the reverse occurs in the other two cases. In other words, the low-level stratification increases the propagation speed, but the upper-level stratification has the opposite effect. This incongruity could be due to the omission of transient gravity waves in the steady-state analytical model. Because the gravity wave activity is suppressed in the shallow stable-layer case, the energy loss due to gravity

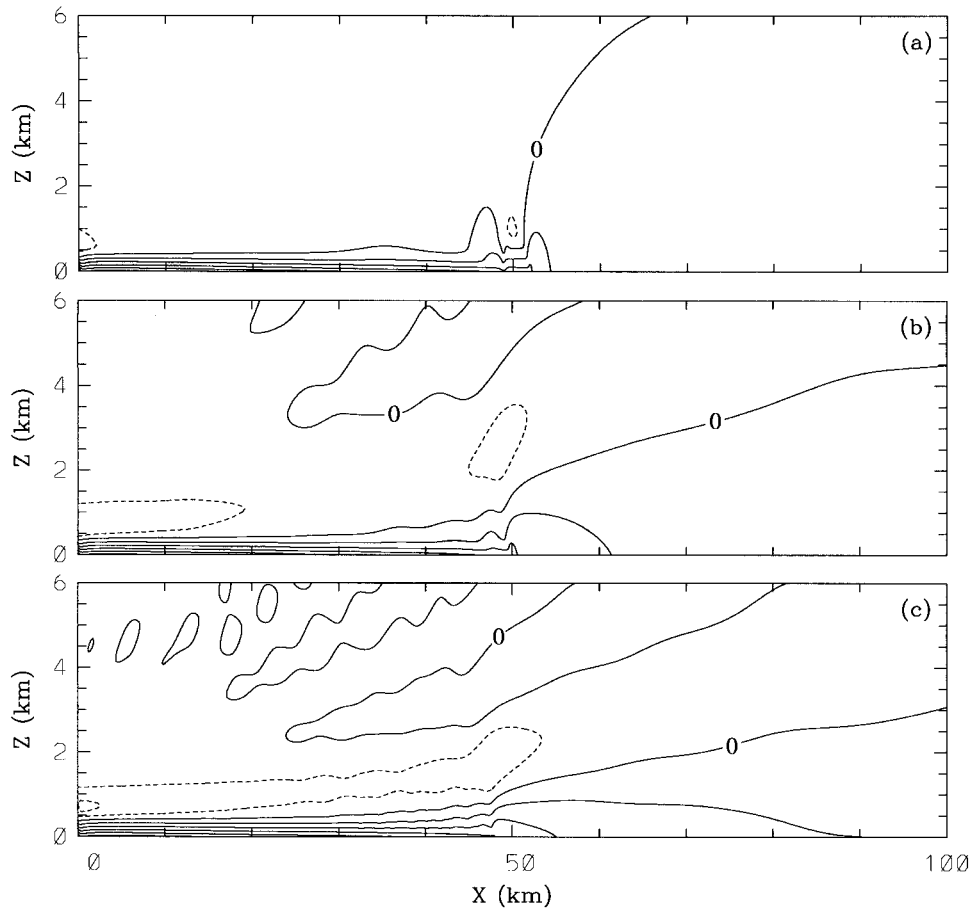

FIG. 16. As in Fig. 14 but for the pressure perturbation. Contour interval is 0.2 mb.

wave radiation is prevented. Consequently, the simulation results are consistent with the analytical model.

According to Haase and Smith (1989), the evolution of density currents intruding into a stable layer is described by the quantity $\mu = c_0/c_{gr}$, the quotient of phase speed of infinitesimal amplitude long waves on a stable layer, and the speed of the equivalent density current in the absence of the stable layer. In terms of this parameter, three distinct regimes can be identified for the stable-layer case. The first regime corresponds to $\mu \lesssim 0.6$, where the modeled system resembles a classical density current. The second regime corresponds to $0.6 < \mu \lesssim 0.9$, where the modeled system is characterized by multiple heads superimposed upon the solitary wave–like disturbances. The third regime corresponds to $\mu > 0.9$, where the foremost head undergoes periodic generation and dissolution and the solitary wave–like disturbance periodically develops around the head and propagates away. These results are broadly comparable to the numerical study by Haase and Smith except that the threshold μ corresponding to their supercritical and subcritical regimes is larger in our simulations.

c. Variation of Froude number with stratification

Figure 18 shows the static stability dependence of the Froude number (F) estimated by the classical density-current propagation formula,

$$C = F\sqrt{g\frac{\Delta\theta}{\theta_0}h}$$

where C is the propagation speed, h the density current height, and $\Delta\theta$ the potential temperature deficit relative to the environmental value θ_0. To estimate F, the propagation speed is calculated from the numerical results. The term inside the radical is computed by integrating the buoyancy field from the surface to the outflow boundary defined by the 0.1 tracer contour. (Note the estimate of F is a lower bound because the temperature perturbations in the current are affected by the adiabatic cooling.)

In the stable-layer case, the Froude number is insensitive to the stratification provided it is not too strong. In the neutral lower-layer case, the Froude number increases with stratification, reaches the maximum at $N = 0.01\ s^{-1}$, and then decreases, but the dependence of

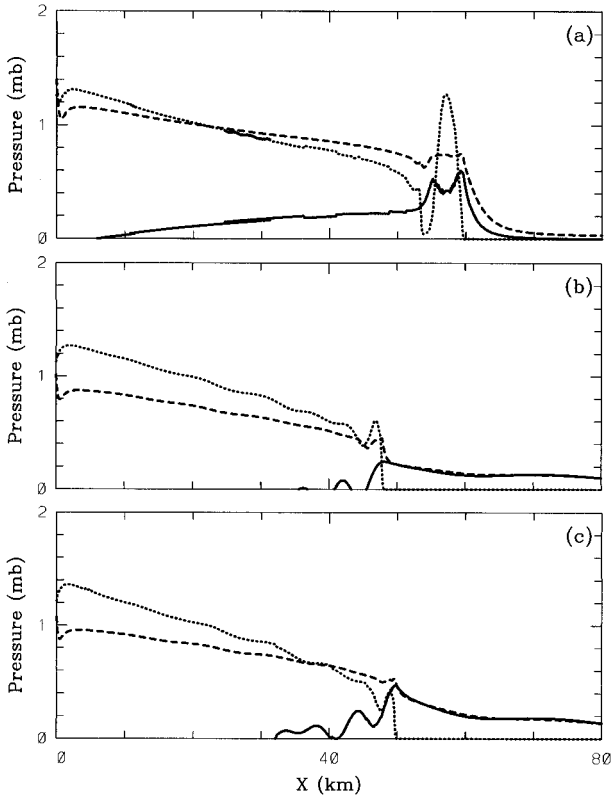

FIG. 17. Hydrostatically generated surface pressure distributions outside the density current (solid line) and inside the density current (dotted line) as well as the surface pressure perturbation (dashed line) at 1.5 h as $N = 0.01\ s^{-1}$. (a) A low-level stable layer, (b) a low-level neutral layer, and (c) a continuously stratified state.

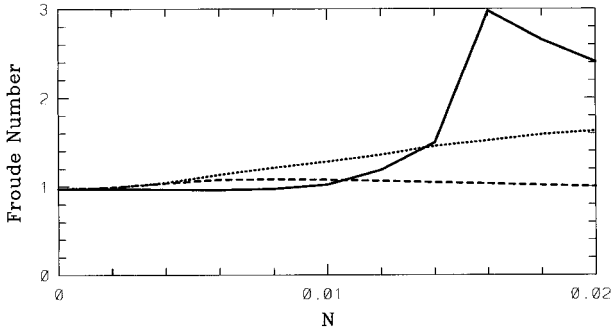

FIG. 18. Variation of the Froude number with stratification. The solid, dashed, and dotted lines correspond to the low-level stable-layer case, the low-level neutral-layer case, and the continuously stratified case, respectively.

the Froude number on the static stability is weak. In the continuously stratified case, the Froude number increases monotonically with stratification, attaining a value of 0.97 at $N = 0$, 1.28 at $N = 0.01\ s^{-1}$, and 1.63 at $N = 0.02\ s^{-1}$. It is concluded that the Froude number is generally larger in stratified flow than in unstratified flow, consistent with the analytical result of Liu and Moncrieff (1996b). We reiterate that in calculating Froude numbers from observations, it is difficult to distinguish the density-current contribution from the effects of adiabatic cooling and latent heating.

8. Conclusions

Stratification affects how laboratory models and density-current theory for unstratified flows are applied to the real atmosphere. Its influence is important, except in special circumstances. We systematically examined the effects of stratification on the structure and propagation of density currents in idealized situations by exploring the response of cold outflow from a fixed cold-air reservoir to various stratified environments. We concentrated on three cases—a shallow stratified layer underlying a deep unstratified layer, a shallow unstratified layer underlying a deep stratified flow, and a continuously stratified state.

In the first case, an idealization of a nocturnal boundary layer, the simulated current system becomes progressively less elevated as the stratification increases, while the corresponding propagation speed progressively increases provided wave disturbances do not move away from the current. The outflow has a dramatic dependence on stratification. In weak stratification, the structure is similar to classical density currents, which have an elevated head and a relatively shallow body. In intermediate stratification the system possesses multiple heads, a variant of the classical density current. In strong stratification, the current system is unsteady and the leading head periodically dissipates and new heads develop. Furthermore, borelike disturbances form around the leading head and propagate away. Similar results have been reported in Crook and Miller (1985), Simpson (1987), and Hasse and Smith (1989).

In the second case, which represents daytime conditions, upper-level stratification reduces both the outflow height and the propagation speed. As expected, the overlying stratification does not significantly change the overall dynamical structure. In other words, the primary variation in structural properties occur in nocturnal conditions.

In the third case, as in the second, stratification flattens the density current and slows its translation. The modeled system maintains the characteristics of laboratory density currents provided the stratification is weak or moderate. In the strongly stratified situation, however, severe head-flattening occurs and the leading current has a wedgelike morphology.

The simulations were compared with the analytical modeling of Liu and Moncrieff (1996b). In general, the variation of current heights with stratification in the theoretical and numerical studies are consistent. However, apart from the stable lower-layer case, the propagation speed increases with stratification in the analytical study but decreases in the numerical simulation for two reasons. First, gravity waves are omitted in the analytical

model. Second, the propagation speed (the surface inflow speed) in the analytic model is normalized by a dimensional quantity that varies case-by-case in the simulations. Nevertheless, a consistent result is that the Froude number in both theoretical and numerical situations increases when stratification is included.

Our results are a basis for interpreting the behavior of density currents in more complex stratification and also for further dynamical studies that take account of ambient flow and vertical shear in a stratified environment following, for example, the numerical and analytic approaches used by Liu and Moncrieff (1996a,b) and Moncrieff and Liu (1999) for unstratified flow.

Acknowledgments. The National Center for Atmospheric Research is sponsored by the National Science Foundation.

REFERENCES

Benjamin, T. B., 1968: Gravity currents and related phenomena. *J. Fluid Mech.,* **31,** 209–248.

Bischoff-Gauss, I., and G. Gross, 1989: Numerical studies on cold fronts. Part I: Gravity flows in a neutral and stratified atmosphere. *Meteor. Atmos. Phys.,* **40,** 150–158.

Chen, C., 1995: Numerical simulations of gravity currents in uniform shear flows. *Mon. Wea. Rev.,* **123,** 3240–3253.

Clark, T. L., 1977: A small-scale dynamic model using a terrain-following coordinate transformation. *J. Comput. Phys.,* **24,** 186–215.

Clarke, R. E., R. K. Smith, and D. G. Reid, 1981: The morning glory of the Gulf of Carpentaria: An atmospheric undular bore. *Mon. Wea. Rev.,* **109,** 1733–1750.

Crook, N. A., 1986: The effect of ambient stratification and moisture on the motion of atmospheric undular bores. *J. Atmos. Sci.,* **43,** 171–181.

——, 1988: Trapping of low-level internal gravity waves. *J. Atmos. Sci.,* **45,** 1533–1541.

——, and M. J. Miller, 1985: A numerical and analytical study of atmospheric undular bores. *Quart. J. Roy. Meteor. Soc.,* **111,** 225–242.

Doviak, R. J., and R. S. Ge, 1984: An atmospheric solitary gust observed with a Doppler radar, a tall tower, and a surface network. *J. Atmos. Sci.,* **41,** 2559–2573.

Droegemeier, K. K., and R. B. Wilhelmson, 1986: Kelvin–Helmholtz instability in a numerically simulated thunderstorm outflow. *Bull. Amer. Meteor. Soc.,* **67,** 416–417.

——, and ——, 1987: Numerical simulation of thunderstorm outflow dynamics. Part I: Outflow sensitivity experiments and turbulence dynamics. *J. Atmos. Sci.,* **44,** 1180–1210.

Haase, S. P., and R. K. Smith, 1989: The numerical simulation of atmospheric gravity currents. Part II: Environments with stable layers. *Geophys. Astrophys. Fluid Dyn.,* **46,** 35–51.

Jin, Y., S. E. Koch, Y.-L. Lin, F. M. Ralph, and C. Chen, 1996: Numerical simulations of an observed gravity current and gravity waves in an environment characterized by complex stratification and shear. *J. Atmos. Sci.,* **53,** 3570–3588.

Liu, C.-H., and M. W. Moncrieff, 1996a: A numerical study of the effects of ambient flow and shear on density currents. *Mon. Wea. Rev.,* **124,** 2282–2303.

——, and ——, 1996b: An analytical study of density currents in sheared, stratified fluids including the effects of latent heating. *J. Atmos. Sci.,* **53,** 3303–3312.

Moncrieff, M. W., and D. W. K. So, 1989: A hydrodynamical theory of conservative bounded density currents. *J. Fluid Mech.,* **198,** 177–197.

——, and C.-H. Liu, 1999: Convection initiation by density currents: Role of convergence, shear, and dynamical organization. *Mon. Wea. Rev.,* **127,** 2455–2464.

Physick, W. L., 1976: A numerical model of the sea-breeze phenomenon over a lake or gulf. *J. Atmos. Sci.,* **33,** 2107–2135.

Raymond, D. J., and R. Rotunno, 1989: Response of a stably stratified flow to cooling. *J. Atmos. Sci.,* **46,** 2830–2837.

Simpson, J. E., 1987: *Gravity Currents in the Environment and Laboratory.* Ellis Horwood Limited, 244 pp.

Smith, R. K., M. J. Reeder, N. J. Tapper, and D. R. Christie, 1995: Central Australian cold fronts. *Mon. Wea. Rev.,* **123,** 16–38.

Thorpe, A. J., M. J. Miller, and M. W. Moncrieff, 1980: Dynamical models of two-dimensional downdraughts. *Quart. J. Roy. Meteor. Soc.,* **106,** 463–484.

Xu, Q., 1992: Density currents in shear flows—A two-fluid model. *J. Atmos. Sci.,* **49,** 511–524.

——, and M. W. Moncrieff, 1994: Density current circulations in shear flows. *J. Atmos. Sci.,* **51,** 434–446.

——, M. Xue, and K. E. Droegemeier, 1996: Numerical simulations of density currents in sheared environments within a vertically confined channel. *J. Atmos. Sci.,* **53,** 770–786.

Xue, M., Q. Xu, and K. E. Droegemeier, 1997: A theoretical and numerical study of density currents in nonconstant shear flows. *J. Atmos. Sci.,* **54,** 1998–2019.